2009 American Control Conference
Hyatt Regency Riverfront, St. Louis, MO, USA
June 10-12, 2009

Active Suspension Control with Direct-Drive Tubular Linear Brushless Permanent-Magnet Motor

Seungho Lee and Won-jong Kim
Department of Mechanical Engineering
Texas A&M University
College Station, Texas 77843, USA

Abstract—**Recently, active suspension has been applied to many commercial automobiles. To develop the control algorithm for active suspension, a quarter-car test bed was built by using a direct-drive tubular linear brushless permanent-magnet motor (LBPMM) as a force-generating component. Modified lead-lag control, linear-quadratic (LQ) servo control with a Kalman filter, the fuzzy control methodologies were implemented for active-suspension control. In the case of fuzzy control, an asymmetric membership function was introduced. This controller could attenuate road disturbance by up to 78%. Both simulation and experimental results are presented to demonstrate the effectiveness of these control methodologies.**

Keywords—**tubular linear actuator, quarter-car, lead-lag control, LQ servo, fuzzy control.**

I. Introduction

Active suspension supports a vehicle and isolates passengers from road disturbances for ride quality and vehicle handling using force-generating components under feedback control. Development of an active-suspension system should be accompanied by the methodologies to control it. Considering costly commercial vehicles with active suspension, Allen constructed a quarter-car test bed to develop the control algorithms [1].

Many researchers developed active-suspension control techniques [2]–[7]. These researches could be categorized according to the applied control theories. When it comes to the LQ control, Peng, *et al*. presented the virtual input signal determined by the LQ optimal theory for active-suspension control [2]. Tang and Zhang applied linear-quadratic-Gaussian (LQG) control, neural networks, and genetic algorithms in an active suspension and presented simulation results [3]. Sam, *et al*. applied LQ control to simulate an active-suspension system [4]. As for the robust control, Lauwerys, *et al*. developed a linear robust controller based on the μ-synthesis for the active suspension of a quarter car [5]. Wang, *et al*. presented the algorithm to reduce the order of the H_∞ controller in the application of active suspension [6]. They were able to reduce the controller's order by nearly one third while the performance was only slightly degraded. Abbas, *et al*. applied sliding-mode control for nonlinear full-vehicle active suspension [7]. They considered not only the dynamics of the nonlinear full-vehicle active-suspension system but also the dynamics of the four actuators.

The LBPMM is directly applicable to active suspension without converting rotary motion to linear motion [8]. Besides its smooth, precise translational motion without cogging, the fact that the length of the mover can be conveniently adjusted makes it appropriate for the force-generating component in an active-suspension system.

Since a human body is most susceptible to vibration at around 3 Hz (20 rad/s) [10], disturbance from the road is modeled as a sinusoidal input with a frequency of 3.5 Hz (22 rad/s) and a magnitude of ±0.03 m in this research. The LBPMM was designed to be able to generate the force up to 29.6 N with a ±6-A phase current [8]. Since NdFeB magnet would lose magnetization around 150°C, control performance is compromised with the maximum current swing that yields temperature rise. As a result, controllers are designed to have the current limit of around ±4 A. The piezoelectric accelerometers (Piezotronics model 336B18) used in the quarter-car test bed also limit the performance. These accelerometers can be used only in the frequency range of 0.5 to 3000 Hz (3 to 20000 rad/s). Particularly, this implies that our active-suspension system is not able to attenuate the disturbance with a frequency component lower than 0.5 Hz.

The fact that the LBPMM is used for active suspension and three different classes of control methodologies are developed and successfully implemented is the key contribution of this research and differentiates this paper from others. Especially, in the case of fuzzy control, an asymmetric fuzzy controller was implemented to compensate for dc offset in sensor data.

This paper is organized as follow. In Section II.A, working principles of the LBPMM are summarized. Section II.B presents the modeling of the quarter-car test bed. In Section III.A, implementation of a modified lead-lag controller and its disturbance attenuation are presented. Section III.B describes the design and performance of an LQ servo controller and the state estimation by a Kalman filter. Section III.C presents a fuzzy controller with asymmetric membership functions and its performance. The conclusions follow in Section IV.

978-1-4244-4524-0/09/$25.00 ©2009 AACC

II. Test Bed for Active Suspension Control

A. Linear Brushless Permanent-Magnet Motor

Fig.1 shows a conceptual configuration of the LBPMM. The mover of the LBPMM consists of a series of cylindrical permanent magnets. The magnets are fixed in a brass tube and connected each other in an NS–NS—SN–SN fashion with spacers between the pairs. The stator consists of 9 coils (3 per each phase).

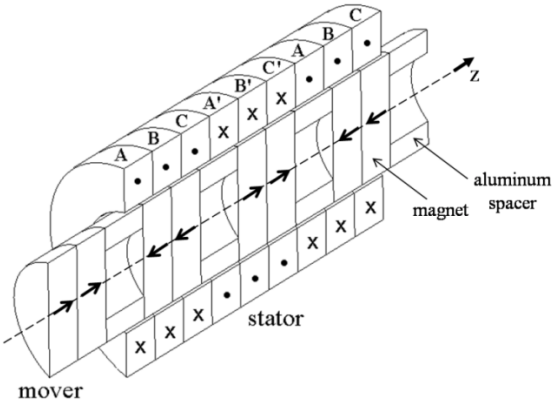

Fig. 1. Schematic diagram of the LBPMM. The direction of the generated force on the mover is in the negative *z*-direction in this particular current distribution.

By the Lorentz force equation, the generated force is the vector cross product of the current density $\boldsymbol{J}$ in the coils and the magnetic flux density $\boldsymbol{B}$ generated by the magnets, $\boldsymbol{F} = \boldsymbol{J} \times \boldsymbol{B}$ [8]. The inverse Blondel-Park transformation in the LBPMM that governs the relationship between the three-phase currents and the desired force is defined as follows [8].

$$\begin{bmatrix} i_a(t) \\ i_b(t) \\ i_c(t) \end{bmatrix} = C \begin{bmatrix} 2 & 0 \\ 1 & \sqrt{3} \\ -1 & \sqrt{3} \end{bmatrix} \begin{bmatrix} \cos \gamma_1 z_o \\ \sin \gamma_1 z_0 \end{bmatrix} f_{zd}(t) \tag{1}$$

where $i_a(t)$, $i_b(t)$, and $i_c(t)$ are the currents flowing in phases A, B, and C, respectively. f_{zd} is the desired force in the axial direction. $\gamma_1 = |2\pi / l|$, where l is the pitch of the motor (63.3 mm). z_0 is relative displacement between the mover and the stator. In active suspension, it is the distance between the sprung and unsprung masses. The inverse force constant C was determined as 0.1383 A/N by experiments [8].

B. Quarter-Car Test Bed

Fig. 2 shows a photograph of the quarter-car test bed. The sprung mass (M_s) is considered to be the body of a car, and the unsprung mass (M_{us}) represents the mass between its suspension and a wheel. As shown in Fig. 2, two masses are connected with a mechanical spring and the LBPMM. The stator of the LBPMM is fixed to the sprung mass and one end of the mover is fixed to the unsprung mass so that the LBPMM force can act on this quarter-car test bed. The rotating cam shown at the bottom of Fig. 2 simulates sinusoidal road disturbance at various frequencies.

As in [9], the states of the quarter-car test bed are defined as $[\dot{x}_s(t) \quad \dot{x}_{us}(t) \quad x_s(t) - x_{us}(t) \quad x_{us}(t) - x_r(t)]^T$, and its dynamics is expressed as the following state-space matrix form.

$$\begin{bmatrix} \ddot{x}_s(t) \\ \ddot{x}_{us}(t) \\ \dot{x}_s(t) - \dot{x}_{us}(t) \\ \dot{x}_{us}(t) - \dot{x}_r(t) \end{bmatrix} = \begin{bmatrix} 0 & 0 & \frac{-k}{M_s} & 0 \\ 0 & \frac{-c_w}{M_{us}} & \frac{k}{M_{us}} & \frac{-k_w}{M_{us}} \\ 1 & -1 & 0 & 0 \\ 0 & 1 & 0 & 0 \end{bmatrix} \begin{bmatrix} \dot{x}_s(t) \\ \dot{x}_{us}(t) \\ x_s(t) - x_{us}(t) \\ x_{us}(t) - x_r(t) \end{bmatrix} + \begin{bmatrix} \frac{1}{M_s} \\ \frac{-1}{M_{us}} \\ 0 \\ 0 \end{bmatrix} F_{act}(t) + \begin{bmatrix} 0 \\ 0 \\ 0 \\ -1 \end{bmatrix} \dot{x}_r(t) \tag{2}$$

where $\dot{x}_s(t)$ and $\dot{x}_{us}(t)$ are the velocities of the sprung and unsprung masses, respectively, $x_r(t)$ is the sinusoidal disturbance generated by the rotating cam, and $F_{act}(t)$ is the force generated by the LBPMM. Additionally, the wheel is modeled by the spring constant k_w and the viscous damping coefficient c_w. The parameter values are given in Table I. The tire is assumed to be made of natural isoprene which has modulus of elasticity of 0.01 GPa.

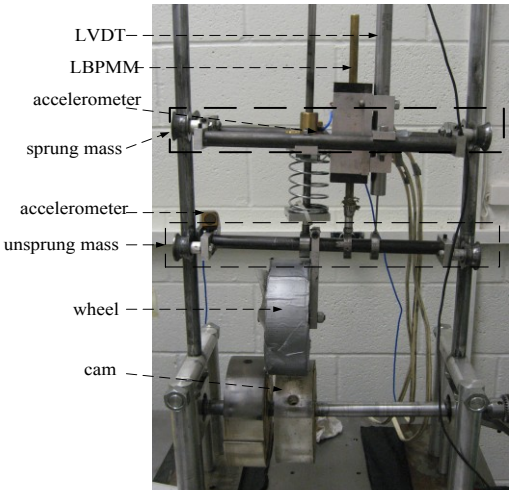

Fig. 2. Photograph of the quarter-car test bed with active suspension.

TABLE I
Parameters and Corresponding Values of Quarter-Car

Parameters	Values
M_s	2.299 kg
M_{us}	2.278 kg
k	1521 N/m
c_w	50 N-s/m
k_w	156 N/m

III. Control Methodologies and Experimental Results

In this Section, three classes of controllers are designed and implemented in the quarter-car test bed and their experimental results are presented.

A. Modified Lead-Lag Control

The output force controls the velocity of the sprung mass rather than its position. From (2) and Table I, the transfer function from $F_{act}(t)$ to $\dot{x}_s(t)$ is determined as follows.

$$G(s)=\frac{0.435s^3+9.547s^2+29.79s+5.831\times10^{-14}}{s^4+21.95s^3+1398s^2+1.452\times10^4 s+4.531\times10^4} \quad (3)$$

The control objectives are as follows. First, high loop gain is desirable around the operating frequency at 22 rad/s for good disturbance attenuation and command following. However, this high gain would yield large current flow in the LBPMM, which would raise its temperature and demagnetize the magnets. Therefore, the gain was limited by examining the simulation result of the maximum current flow (±4 A) in the LBPMM. Finally, the loop gain of the controller at around the operating frequency was determined as 56 dB.

Second, the control bandwidth was set to be [10 rad/s, 80 rad/s]. Since the open-loop frequency response of this quarter car has low gain in low and high frequencies and high gain in the middle frequency with two cross-over frequencies, the bandwidth could be adjusted by changing either the lower cross-over frequency or the higher cross-over frequency. In this paper, a lag compensation $(0.2252s+1.15)/(s+1.005)$ was applied in the low-frequency range to achieve this goal.

Third, since the gain should be low in the high frequency range to attenuate noise, another lag compensation $(0.04681s+100.5)/(s+100.54)$ was applied. Finally, sufficient gain and phase margins should be obtained due to modeling uncertainties. To achieve this objective, a lead compensation $(1.949s+100)/(s+100.02)$ was introduced between the two lag controllers.

The lower-frequency lag controller yields a lower loop gain. The lead controller around the operating frequency broadens the bandwidth. Therefore, each lead or lag controller should be fine-tuned by examining the overall loop transfer function. To decide the exact corner frequencies in each of the lead or lag controllers, the Matlab SISO (single-input-single-output) tool was used. The modified lead-lag controller with one lead and two lag controllers was finalized in the *s* domain as (4). Fig. 3 shows the frequency response of the loop transfer function.

As seen from Fig. 3, the loop-transfer-function gain is higher than that of the quarter-car transfer function around the operating frequency (22 rad/s). The bandwidth is acceptable since it is close to the frequency range of [10 rad/s, 80 rad/s].

The simulation and experimental results of disturbance rejection are presented in Fig. 4.

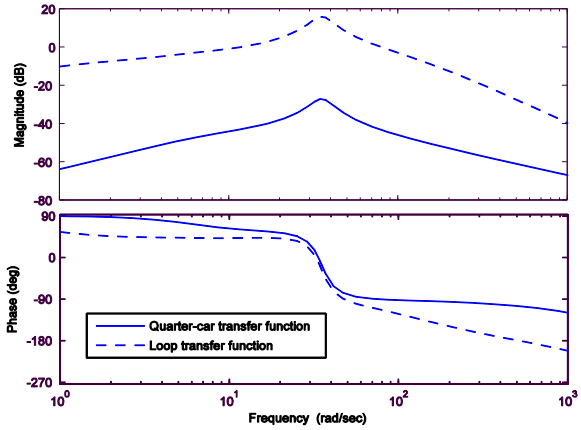

Fig. 3. Quarter-car and loop-transfer-function frequency responses of the quarter-car dynamics (3) and the modified lead-lag controller (4). Gain and phase margins are 28.2 dB and 66.4°, respectively.

$$C(s)=12\frac{(s+2147)(s+51.31)(s+5.107)}{(s+100.54)(s+100.02)(s+1.005)} \quad (4)$$

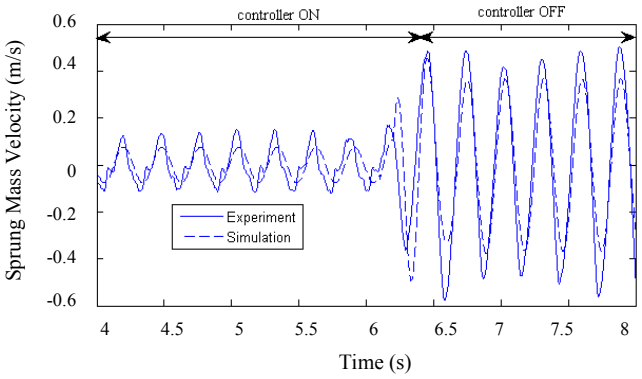

Fig. 4. Experiment and simulation results of the modified lead-lag control for the 3.5 Hz disturbance.

B. Linear-Quadratic Servo Control

LQ servo control is developed by introducing the command input and the output disturbance. From (2), quarter-car model can be expressed as follows.

$$\begin{aligned}\dot{\boldsymbol{x}}_{\boldsymbol{p}}(t)&=A_p\boldsymbol{x}_{\boldsymbol{p}}(t)+B_p u(t)\\ y_p(t)&=C_p\boldsymbol{x}_{\boldsymbol{p}}(t)\end{aligned} \quad (5)$$

where $\boldsymbol{x}_{\boldsymbol{p}}(t)=\begin{bmatrix}\dot{x}_s(t) & \dot{x}_{us}(t) & x_s(t)-x_{us}(t) & x_{us}(t)-x_r(t)\end{bmatrix}^T$,

$A_p=\begin{bmatrix}0 & 0 & \frac{-k}{M_s} & 0\\ 0 & \frac{-c_w}{M_{us}} & \frac{k}{M_{us}} & \frac{-k_w}{M_{us}}\\ 1 & -1 & 0 & 0\\ 0 & 1 & 0 & 0\end{bmatrix}$, $B_p=\begin{bmatrix}\frac{1}{M_s}\\ \frac{-1}{M_{us}}\\ 0\\ 0\end{bmatrix}$, $C_p=\begin{bmatrix}1\\0\\0\\0\end{bmatrix}^T$ as in (2)

Thus, $y_p(t)=\dot{x}_s(t)$, and $\boldsymbol{x}_{\boldsymbol{p}}(t)$ is partitioned as follows.

$$\boldsymbol{x_p}(t) = \left[y_p(t) \,|\, \boldsymbol{x_R}^T(t) \right]^T$$
$$= \left[\dot{x}_s(t) \,|\, \dot{x}_{us}(t) \quad x_s(t) - x_{us}(t) \quad x_{us}(t) - x_r(t) \right]^T \quad (6)$$

The vertical line indicates that $y_p(t) = \dot{x}_s(t)$.

As shown in Fig. 5, the control gain matrices G_y and G_r are applied to $y_p(s)$ and $\boldsymbol{x_R}(s)$, respectively. To eliminate a non-zero steady-state error for the step command input or the output disturbance, this LQ servo controller is implemented with an integrator. In this application, the LQ servo model is determined by considering the frequency responses of the loop transfer function of model given in Fig. 5.

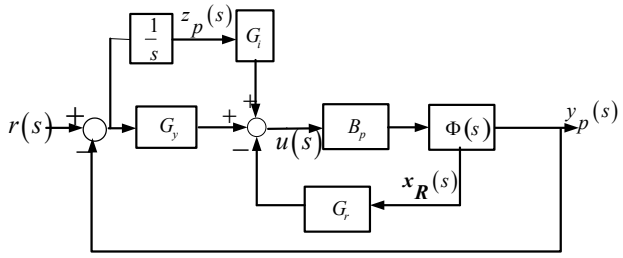

Fig. 5. Block diagrams of LQ servo control in this application.

The control objectives are similar to those of the modified lead-lag control. As shown in Fig. 5, the control gains for the integrator, output state, and rest states are G_i, G_y, G_r, respectively [11]. This LQ servo system consisted of the standard LQ servo dynamics (5) and the integrator dynamics. With $r(s) = 0$ in a regulation problem,

$$z_p(s) = -\frac{I}{s} y_p(s) = -\frac{I}{s} \dot{x}_s(s). \quad (7)$$

The augmented system is defined as follows.

$$\dot{\boldsymbol{x}}(t) = A\boldsymbol{x}(t) + Bu(t), \quad (8)$$

where $\boldsymbol{x}(t) = \left[z_p(t) \; y_p(t) \; \boldsymbol{x_R}^T(t) \right]^T$, $A = \begin{bmatrix} 0 & -C_P \\ 0 & A_P \end{bmatrix}$ and $B = \left[0 \quad B_p{}^T \right]^T$. The control law is defined as follows.

$$u(t) = -G\boldsymbol{x}(t), \quad (9)$$

where $G = \left[G_i \quad G_y \quad G_r \right]$.

To obtain G, a control algebric Riccati equation (CARE) should be solved. To construct this CARE, a symmetric positive definite matrix R and a symmetric positive semi-definite matrix Q should be determined. The R matrix affects the loop gain that determines the system bandwidth. After several design iterations, R was set to be 0.005. The diagonal elements of the Q matrix are the weights of each state, after several design iterations, the Q matrix was determined as follows.

$$diag(Q) = \left[0.01 \quad 170 \quad 0.01 \quad 0.01 \quad 0.01 \right]$$
$$Q_{ij} = 0 \text{ for } i \neq j \quad (10)$$

A unique positive semi-definite symmetric matrix K is determined by the following CARE.

$$-KA - A^T K - Q + KBR^{-1}B^T K = 0 \quad (11)$$

K is solved with Matlab as follows.

$$K = \begin{bmatrix} 1.1078 & 0 & 0 & -1.1078 & -1.1078 \\ 0 & 0 & 0 & -0.0003 & 0 \\ 0 & 0 & 0 & -0.0003 & 0 \\ -1.1078 & -0.0003 & -0.0003 & 1.1190 & 1.1104 \\ -1.1078 & 0 & 0 & 1.1104 & 1.1102 \end{bmatrix} \quad (12)$$

The feedback gain G is determined as follows.

$$G = R^{-1}BK = \left[0.0013 \quad 147.58 \quad -25.72 \quad 0 \quad 272.54 \right] \quad (13)$$

1) Kalman Filter Design

LQ servo requires full state feedback. The last state of the system is defined as the tire deflection ($x_{us}(t) - x_r(t)$) which is difficult to be measured because locating any type of the sensor in the rotating wheel is inconvenient. Therefore, it is estimated by a Kalman filter. To solve the filter algebric riccati equation (FARE) and obtain the Kalman filter gain, a positive value Θ and a non-negative value Ξ should be determined in (15). They are adjusted and determined as $\Theta = 0.00001$ and $\Xi = 0.01$ after several design iterations. The disturbance matrix L defined as follows.

$$L = \left[0 \quad 0 \quad 0 \quad -1 \right]^T \quad (14)$$

Then the unique positive semi-definite symmetric matrix P is determined by solving the following FARE.

$$AP + PA^T + L\Xi L^T - PC^T\Theta^{-1}CP = 0 \quad (15)$$

The solution is obtained as follows by Matlab 'CARE' function.

$$P = \begin{bmatrix} 0.0005 & 0.0004 & 0 & -0.0003 \\ 0.0004 & 0.0012 & 0 & -0.0008 \\ 0 & 0 & 0 & 0 \\ -0.0003 & -0.0008 & 0 & 0.0007 \end{bmatrix} \quad (16)$$

The Kalman filter gain H is determined as follow.

$$H = PC^T\Theta^{-1} = \left[46.92 \quad 41.96 \quad -1.66 \quad -28.97 \right] \quad (17)$$

Fig. 6 shows the estimated tire deflection ($x_{us}(t) - x_r(t)$) by the Kalman filter algorithm in closed-loop control. The solid line represents the estimated state generated from Control Desk during the experiment. The dashed line represents the

estimated state generated from the Simulink block without the experiment setup. There is some discrepancy between the simulation and experimental results of state estimation. In the Kalman filter algorithm, the measured output and the disturbance are assumed as zero-mean white Gaussian noises. In the quarter-car model, there is some discrepancy between the measured output ($\dot{x}_s(t)$) and the zero-mean white Gaussian noise (Figs. 4 and 7), which limits the performance of the state estimator. Noises from three sensors also degrade the performance of the state estimator.

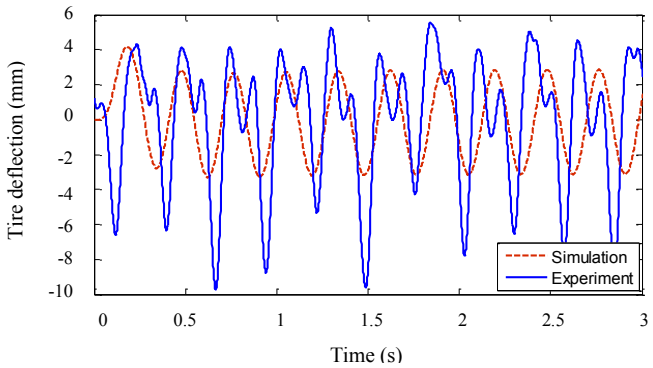

Fig. 6. Estimated state comparison between simulation and experiment results.

The performance of the disturbance attenuation is presented in Fig. 7. Due to the error from the state estimator, disturbance attenuation contains some discrepancy between the experiment and simulation results.

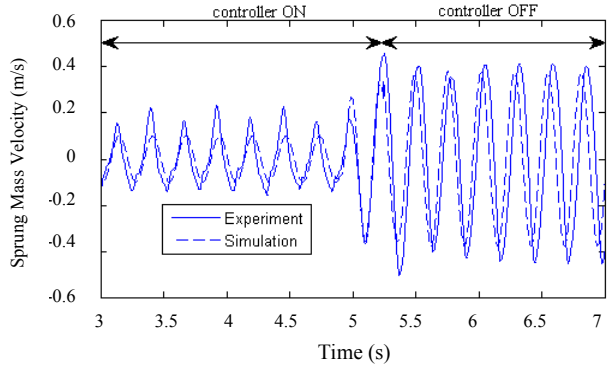

Fig. 7. Experiment and simulation results of the LQ servo control when the controller is turned on.

C. Fuzzy Control

A Mamdani-type fuzzy controller is implemented in this section [12]. The input to this fuzzy controller is the system error ($e(t)$), and the output is the control input ($F_{act}(t)$). To determine $F_{act}(t)$, $e(t)$ is fuzzified by the membership functions shown in Fig. 8 (a) and defuzzified by the membership functions shown in Fig. 8 (b). The area under the membership functions are defined by μ_i ($i = 1, 2, \cdots, 7$).

The range of error in Fig. 8 (a) was set as [–0.8, 0.8] because the magnitude of the largest measured error ($|\dot{x}_s(t)|$) was 0.8 m/s. The range of outputs in Fig. 8 (b) was set as [–30, 30] because the LBPMM could generate force up to near ±30 N.

Since this active-suspension test bed is a single-input, single-output system, the input and the output from single-dimension arrays. Each fuzzified value is one-to-one matched for the defuzzification. For example, if the error is NLE, the output is NLF. Each rule has the same weight.

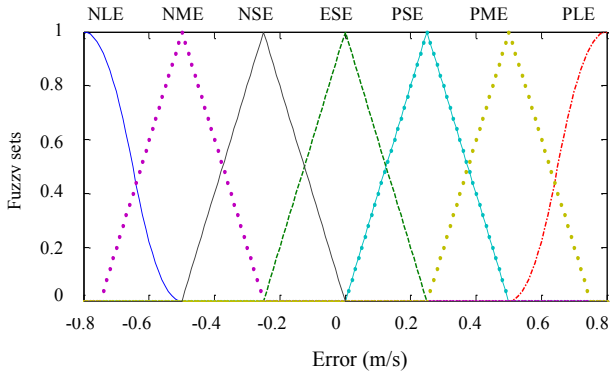

(a)

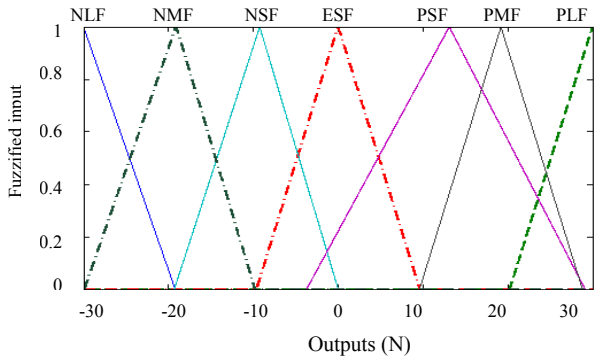

(b)

Fig. 8. (a) Membership functions for fuzzification. (b) Membership functions for defuzzification.

The control input as the result of this fuzzy controller is determined by the center of gravity (COG) method. The COG method computes F_{act} as follows [12].

$$F_{act} = \sum_{i=1}^{7} g_i \int \mu_i \Big/ \sum_{i=1}^{7} \int \mu_i \ , \qquad (18)$$

where g_i is defined as the COG of the each membership function.

Fig. 9 shows the relation between the error and the generated control force. This input-output curve was designed not to be symmetric with respect to the origin. When the active-suspension system is under closed-loop control, the sprung mass's maximum absolute velocity is larger when its velocity is positive compared to that with a negative velocity. This phenomenon was examined through the modified lead-lag control and the LQ servo control (Figs. 4 and 7).

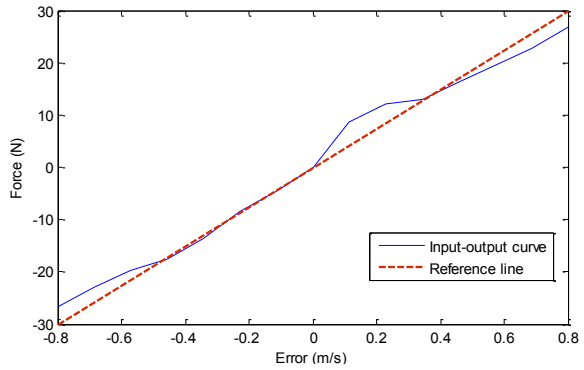

Fig. 9. Input-output relation of the asymmetric fuzzy controller.

This phenomenon indicates that the position of the sprung mass is higher than the desired position and its insufficient control. Therefore, additional control input should be generated. To solve the problem, a membership function PSF in Fig. 8 (b) was widened. In Fig. 10, this phenomenon is reduced in comparison with Figs. 4 and 7 due to the additional control input generated in the hump where 0.1 < Error (m/s) < 0.4 in Fig. 9.

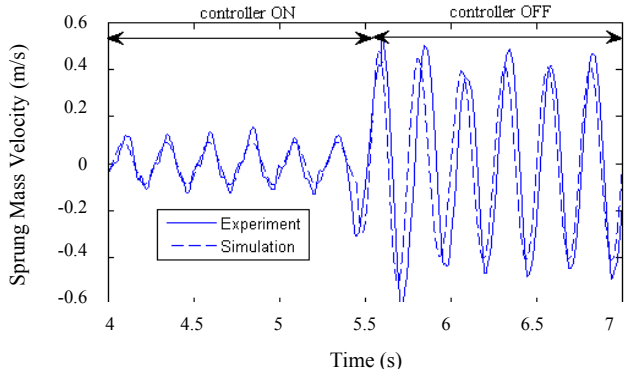

Fig. 10. Fuzzy control result of experiment and simulation when controller is turned on.

IV. Conclusions

An active-suspension system with a quarter-car test bed was constructed with an LBPMM in this research. Modified lead-lag, LQ servo, fuzzy controllers were designed and implemented to attenuate modeled road disturbance. The fuzzy controller was able to reject the disturbance by up to 78%.

The LQ servo's performance in disturbance rejection was slightly inferior to the two other controllers. The reason is that the estimator could not perfectly generate the estimated state because the noise and the disturbance were not zero-mean white Gaussian. Moreover, an additional sensor (the LVDT) was used in this control method. The performance of the modified lead-lag control was fairly acceptable. The fuzzy controller turned out to be the most suitable control methodology for this active-suspension application. It is because its asymmetric membership functions allowed the LBPMM to generate the most suitable control force. Due to the asymmetric membership functions, the discrepancy between the ideal and practical test beds was reduced. However, a fuzzy controller is difficult to design since it has infinitely many design parameters such as selecting the domain for the fuzzification and defuzzyfication. In this research, these design parameters were finalized with the results from the modified lead-lag and LQ servo controllers.

References

[1] J. Allen, *Design of Active Suspension Control Based Upon Use of Tubular Linear Motor and Quarter-Car Model*, Master's Thesis, Texas A&M University, August 2008.

[2] H. Peng, R. Stratharn, and A. Ulsoy, "A Novel Active Suspension Design Technique–Simulation and Experimental Results," *Proceedings of 1997 American Control Conference*, pp. 709–713, June 1997.

[3] C. Tang and T. Zhang, "The Research on Control Algorithms of Vehicle Active Suspension System," *Proceedings of IEEE International Conference on Vehicular Electronics and Safety*, pp. 320–325, October 2005.

[4] Y. M. Sam, M. R. H. A. Ghani, and N. Ahmad, "LQR Controller for Active Car Suspension," *Proceedings of TENCON 2000*, pp. 441–444, September 2000.

[5] C. Lauwerys, J. Swevers, and P. Sas, "Design and Experimental Validation of a Linear Robust Controller for an Active Suspension of a Quarter-car," *Proceedings of 2004 American Control Conference*, pp. 1481–1486, July 2004.

[6] J. Wang, A. C. Zolas, and D. A. Wilson, "Active Suspension: A reduced-Order H_∞ Control Design Study," *Proceedings of Mediterranean Conference on Control and Automation*, pp. 132–140, July 2007.

[7] C. Abbas, T. Rahaijaona, and H. Noura, "Sliding Mode Control Applied to Active Suspension Using Nonlinear Full Vehicle and Actuator Dynamics," *Proceedings of 2006 IEEE conference on Decision and Control*, pp. 3597–3602, December 2006.

[8] W.-J. Kim and B. Murphy, "Development of a Novel Direct-Drive Tubular Linear Brushless Permanent-Magnet Motor," *International Journal of Control, Automation, and System*, vol. 2, no. 3, pp. 279–288, September 2004.

[9] R. Rajamani, "Adaptive Observers for Active Automotive Suspensions: Theory and Experiment," *IEEE Transactions on Control Systems Technology,* vol. 3, no. 1, pp. 86–93, March 1995.

[10] G. Stein, "Respect the Unstable," *IEEE Control Systems Magazine*, vol. 23, no. 4, p. 12–25, August 2003.

[11] B. Anderson and J. Moore, *Optimal Control: Linear Quadratic Methods*, Prentice-Hall, p. 74, 1989.

[12] K. Passino and S. Yurkovich, Fuzzy *Control*, Addison-Weslsy, p. 42, 1999.